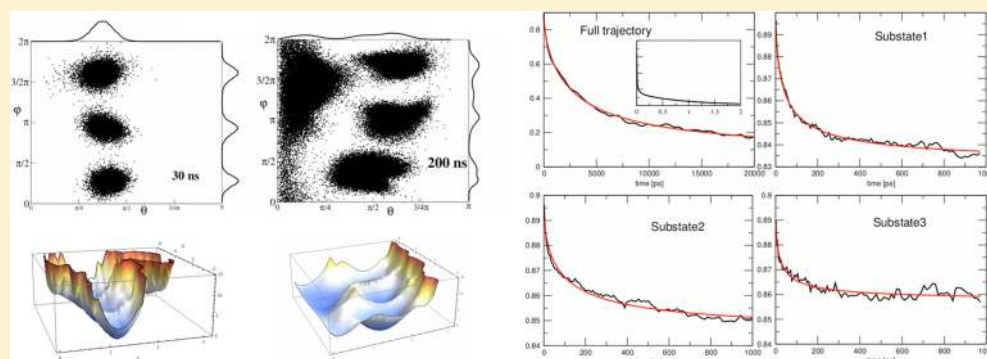# Toward the Characterization of Fractional Stochastic Processes Underlying Methyl Dynamics in Proteins

Paolo Calligari and Daniel Abergel*

Ecole Normale Supérieure, Departement de Chimie, UMR 7203 CNRS-UPMC-ENS, 24, rue Lhomond, 75005 Paris, France

S *Supporting Information*

ABSTRACT: In this article, we investigate the multiple-scale structure of methyl side chain dynamics in proteins. We show that the orientational correlation functions of CH_3 methyl groups are well described by a fractional Brownian dynamics model. Typical angular correlation functions involved in NMR relaxation were computed from MD simulations performed on two different proteins. These correlation functions were shown to be very well fitted by a fractional Ornstein–Uhlenbeck process in the presence of effective local potentials at the C–H and C–C methyl bonds. In addition, our analysis highlights the presence of the asymptotic power law decay of the waiting time probability density of the stochastic process involved, thereby illustrating the connection between approaches based on fractional diffusion equations and the continuous time random walk.

I. INTRODUCTION

Internal motions in proteins have been recognized as an essential ingredient of their functions, in addition to the well-known role played by their three-dimensional structures. In order to study these dynamical aspects, nuclear magnetic resonance (NMR) spectroscopy has emerged as a unique tool allowing one to probe processes taking place on the pico- to millisecond time scale via the measurement of spin relaxation rates.[18] Thus, backbone as well as side chain dynamics, where the functional implication of methyl groups has been largely discussed (for a review, see ref 16), can be investigated. The dynamics of methyl groups in proteins on fast time scales, i.e., in the subnanosecond range, is extremely rich. Moreover, it is also rather complex, which makes it more difficult to analyze and interpret NMR relaxation measurements in terms of pertinent dynamical variables. Thus, various assumptions must be made, regarding the geometry of the methyl group, potential symmetry of the methyl axis motions, or time scale separation between axis and about axis motions, which are typical of model-free-like approaches.[7,23,26,27,32,37] However important, these points do not represent the main subject of this article. Here, we will be concerned with the structure of the underlying stochastic process that drives the bond vector motions and eventually leads to the process of spin relaxation, rather than with the geometrical aspects of their motions. We will show, based on MD simulations, that a certain kind of non-Markovian stochastic process can be assumed, which

reflects the effect of a complex local environment on the diffusion process at work.

Some time ago, it was suggested that internal dynamics in proteins could be characterized by asymptotic power-law decays of correlation functions and could be idealized as fractional stochastic dynamics[14,20,21] or continuous time random walk (CTRW) processes.[14,31] Time self-similarity of backbone protein dynamics was also recently investigated based on MD computations.[9] Such models give rise to correlation functions characterized by a superposition of exponential functions with a broad and continuous distribution of relaxation times.

MD simulations actually represent an attractive method against which a model can be tested in order to get deeper insight into the details of the underlying dynamical processes. In this context, we recently introduced a fractional Brownian dynamics (fBD) approach in the perspective of NMR spectroscopy, which focused on the description of fast backbone dynamics in proteins on the picosecond–nanosecond time scale.[3,4,6] Using MD simulations, we were able to show that the relevant amide NH bond angular correlation functions for NMR relaxation could be well reproduced by a simple fractionnal Ornstein–Uhlenbeck (fOU) diffusion process in a harmonic

potential.[4,6] Based on the analysis of these MD simulations, we also suggested the possibility to use this approach to analyze experimental relaxation rates.[6]

In this article, we investigate the possibility to describe the motions of methyl groups, represented by CH and CC bond vectors, through a fBD approach, based on MD simulations. We show that methyl CH and CC bond vector angular autocorrelation functions can be described in the framework of fractional diffusion in harmonic or multiple-well potentials. To this aim, we analyzed the motions of methyl groups computed from all-atom MD simulations of two proteins, ubiquitin and matrix metalloproteinase-12 (MMP-12). Our results clearly show the multiple time scale character of bond vector fluctuations, occurring even in the fast, pico- to nanosecond range. Specifically, bond vector internal correlation functions were fitted by the kind of Mittag–Leffler (ML) functions that are typically involved in solutions of fractional Fokker–Planck diffusion equations, showing excellent agreement. More importantly, in this context where the local potentials at the methyl groups have complex shapes and the harmonic approximation may not be justified, the correlation functions of the bond vectors are well accounted for by a single ML function that depends on a characteristic time. Moreover, we were able to establish in specific cases the connection between ML decays of the correlation functions and the statistics of the underlying process, as described in the CTRW theory.[31,36] Namely, waiting time probability density functions (pdf) with power law decays could be extracted from the MD trajectories, thereby confirming the fractional Brownian dynamics process at a more fundamental level.

II. METHODS

A. Review of the Theory. In complex systems, relaxation may be characterized by fractional dynamics, which has been evidenced by several techniques, such as fluorescence correlation spectroscopy or kinetic studies.[14,22,28] This kind of dynamics has been shown to be already present on the nanosecond time scale in quasielastic neutron scattering (QENS) and MD simulations studies of proteins.[20,21] At the microscopic level, it can be interpreted as the consequence of energetic obstacles and traps that slow down translation and/or rotation of the diffusing particle and is described by a CTRW, where the waiting time probability distribution function has a power law time dependence. This leads to a diverging first moment of the waiting time, which therefore does not permit the definition of a time scale of the random process,[31] in contrast to Brownian diffusion.

At a different level of description, this process introduces memory effects into the motion[36] which can be described by a fractional diffusion equation.[1] This approach can be formulated for rotational diffusion, which is relevant for dielectric relaxation[19] and NMR.[3,4,6] For a potential of arbitrary shape, the appropriate fractional Fokker–Planck equation (FFPE) for the probability density function $P(\theta, \phi)$ as a function of the polar angles in a molecule fixed frame gives

$$\frac{\partial}{\partial t}P(\theta, \phi) = \tau^{1-\alpha} \, _0D_t^{1-\alpha} L \, P(\theta, \phi) \tag{1}$$

where L is the Fokker–Planck operator in spherical coordinates,[19,31] $0 < \alpha \leq 1$, τ has the dimension of time, and $_0D_t^{1-\alpha}$ is the fractional derivation operator

$$_0D_t^{1-\alpha}f(t) = \frac{1}{\Gamma(\alpha)}\frac{d}{dt}\int_0^t [t - t']^{\alpha-1}f(t') \, dt' \tag{2}$$

where $\Gamma(.)$ is the Gamma function. One of the practical advantages of the fBD approach is its ability to take into account the presence of multiple time scales with a limited and fixed number of parameters, as was recently demonstrated on ^{15}N spin relaxation.[3,4,6] In this approach, internal motions are statistically independent of global tumbling of the protein, which is safely assumed for methyl groups. Therefore the total correlation function $C(t)$ factorizes into the correlation functions $C_I(t)$ and $C_g(t)$ of internal and isotropic global motions: $C(t) = C_g(t)C_I(t)$. In the case of fOU process, $C_I(t)$ can be expressed in terms of a single Mittag–Leffler (ML) function $E_\alpha(-[t/\tau]^\alpha)$ through the expression[3,4,6]

$$C_I = S^2 + (c_{el} - S^2)E_\alpha(-[t/\tau]^\alpha) \tag{3}$$

where the squared-order parameter S^2 is defined as

$$S^2 = \lim_{t\to\infty} C_I(t) = \lim_{t\to\infty} \frac{4\pi}{5}\sum_{m=-2}^{2}\langle Y_{2m}(\theta, \phi)_t Y_{2m}^*(\theta, \phi)_0\rangle \tag{4}$$

Here, $Y_{2m}(\theta, \phi)$ are the second-order spherical harmonics which are relevant to the interaction. The ML function

$$E_\alpha(z) = \sum_{k=0}^{\infty}\frac{z^k}{\Gamma(1 + \alpha k)} \tag{5}$$

is an entire function in the domain of complex numbers.[11] For $0 < \alpha \leq 1$, the stretched ML function in eq 3 can be expressed as the continuous superposition of exponential relaxation functions $\exp(-\lambda t)$, with the relaxation rate distribution function $p_{\alpha,\tau}(\lambda)$

$$E_\alpha(-[t/\tau]^\alpha) = \int_0^{\infty} d\lambda p_{\alpha,\tau}(\lambda) \exp(-\lambda t) \tag{6}$$

The spectrum of relaxation rates is positive and has the form[14,20]

$$p_{\alpha,\tau}(\lambda) = \frac{\tau}{\pi}\frac{(\tau\lambda)^{\alpha-1}\sin(\pi\alpha)}{(\tau\lambda)^{2\alpha} + 2(\tau\lambda)^\alpha\cos(\pi\alpha) + 1} \tag{7}$$

with the normalization condition $\int_0^{\infty}d\lambda \, p_{\alpha,\tau}(\lambda) = 1$. The scaling parameter τ is related to the median $\lambda_{1/2}$ of $p_{\alpha,\tau}(\lambda)$ through $\lambda_{1/2} = \tau^{-1}$.[3] For $\alpha = 1$, $p_{\alpha,\tau}(\lambda)$ reduces to a Dirac distribution centered at the value τ^{-1} and the ML function reduces to an exponential, whereas for $0 < \alpha < 1$ it exhibits a power law decay at long times. This is characteristic of non-Markovian processes with power law memory kernels. Note that in practice, however, it could be possible in some cases to replace the continuous decomposition of the ML function onto the exponential basis, given by $p_{\alpha,\tau}(\lambda)$, by a discrete approximation thereof, and represent the correlation functions as sums of multiple Lorentzians (in the sense of discrete sums). However, in this approximation of $p_{\alpha,\tau}(\lambda)$, the meaning of the α, τ parameters and of the underlying physical model would be completely lost.

The parameter c_{el}, $S^2 < c_{el} < 1$, appearing in eq 3 was introduced[4,6] in order to account for the presence of initial rapidly damped oscillations, which occur for time lags typically shorter than ≈ 1 ps. These are commonly observed in MD simulations and attributed to the presence of very fast dynamical processes. c_{el} therefore represents the value of the correlation function at the minimum time lag where the theory is assumed valid (~ 1 ps). Finally, the spectral density function associated with eqs 3, 6, and 7 is given by[4]

$$J(\omega) = \frac{S^2\tau_0}{1 + (\omega\tau_0)^2}$$
$$+ (c_{el} - S^2)\frac{1}{\gamma}\frac{(\gamma\tau)^\alpha \cos\beta + \cos[\beta(1 - \alpha)]}{(\gamma\tau)^\alpha + (\gamma\tau)^{-\alpha} + 2\cos\beta\alpha} \tag{8}$$

where $\cos\beta = (\tau_0\gamma)^{-1}$, $\sin\beta = \omega/\gamma$, and $\gamma = (\tau_0^{-2} + \omega^2)^{1/2}$.

For a potential of arbitrary shape, eq 1 can be formally solved by using the separation ansatz: $P(\theta, \phi) = \sum_{n=0}^{\infty} \Phi_n(\theta, \phi) T_n(t)$. The decay and spatial modes satisfy the equations[31]

$$\frac{d}{dt}T_n(t) = -\lambda_{n,\alpha 0}D_t^{1-\alpha}T_n(t) \tag{9}$$

$$L\Phi_n(\theta, \phi) = -\lambda_{n,\alpha}\Phi_n(\theta, \phi) \tag{10}$$

where $\lambda_{n,\alpha} = \lambda_n\tau^{1-\alpha}$ and λ_n are the eigenmodes of the Fokker–Plank operator L. The decay modes are thus the ML functions: $T_n(t) = E_\alpha[-\lambda_{n,\alpha}t^\alpha] = E_\alpha[-\lambda_n\tau(t/\tau)^\alpha]$. It is then straightforward to show that, in analogy with eq 3, the part of the correlation function that decays to zero, $\delta C_I(t) = (C_I(t) - S^2)/(c_{e1} - S^2)$, is a superposition of ML functions of the various modes:

$$\delta C_I(t) = \sum_n a_n E_\alpha[-\lambda_n\tau(t/\tau)^\alpha] \tag{11}$$

In some favorable cases, it may be useful to approximate the exact correlation function by a single ML decay with an effective eigenmode as $\delta C_I(t) \approx E_\alpha[-\lambda_{eff}\tau(t/\tau)^\alpha]$. Thus, defining $\tau_{eff}^{-\alpha} = \lambda_{eff}\tau^{1-\alpha}$, one gets from eq 3

$$C_I = S^2 + (c_{el} - S^2)E_\alpha(-[t/\tau_{eff}]^\alpha) \tag{12}$$

B. Computations. *1. MD Simulations.* MD simulations of ubiquitin and MMP-12 were performed with the NAMD program package,[34] starting from their respective NMR and X-ray structures (PDB entries 1D3Z and 2OXU). The all-atom force fields (AMBER99SB[15] for ubiquitin and CHARMM27[30] for MMP-12) were used with periodic boundary conditions. These two different force fields were used to confirm that the fractional character of the stochastic processes is observed, irrespective of the details of the potential. This is expected, as fractionarity is a consequence of the complex, heterogeneous, local environment in which fluctuations take place. Electrostatic interactions were computed by using the PME method[10,12] with a fourth-order B-spline interpolation over a 1 Å-spaced grid. The integration time step was set to 1 fs, and coordinates were saved every 0.5 ps (ubiquitin) or 1 ps (MMP-12). The water models used were SPC/E and TIP3P for ubiquitin and MMP12, respectively. Bond lengths involving H atoms were not constrained during the simulations; therefore, no fixed geometries were assumed for the methyl groups. After a preliminary minimization of the PDB structure, all simulations were first equilibrated at constant temperature (298 K) and constant pressure (1 bar) using a Langevin thermostat[17] coupled with a Nosé–Hoover barostat.[13] The damping coefficient for the Langevin thermostat was 2.5 ps^{-1}. The obtained equilibrated system will be used as starting point for the production runs: 50 ns for ubiquitin and 200 ns for MMP-12.

2. Correlation Function Computation and Fitting. Internal angular correlation functions were calculated using the formula

$$C_I(t) = \frac{1}{T_{MD}}\int_0^{T_{MD}} P_2(u(t)\cdot u(t - \tau))\,d\tau \tag{13}$$

where $P_2(.)$ is a second-order Legendre polynomial, T_{MD} is the total trajectory length, and $\mathbf{u}(t)$ is the unit vector corresponding to the bond vector orientation at time t. It is worth noting that here the average over time is equivalent to an ensemble average based on the ergodic hypothesis.

Internal rotational correlation functions of C−H bond vectors were thus computed from the MD trajectories.[5]

The maximum time lag t_m up to which the correlation functions can be computed with good enough statistics corresponds to the first $\approx 10\%$ of the total trajectory length.[39] Whenever $C_I(t)$ did not reach a plateau value within t_m, or when the plateau value $C_I(\infty)$ of the internal correlation function remained significantly different from the value of S_{MD}^2 ($|C_I(\infty) - S_{MD}^2| \geq 0.1$), insufficient sampling of internal motions during the 50 ns trajectory[33] was assumed, and $C_I(t)$ was discarded from further analysis.

Order parameters S_{MD}^2 were computed by direct implementation of the following equation

$$S^2 = \frac{4\pi}{5}\sum_{m=-2}^{2}\langle Y_{2m}(\theta, \phi)\rangle\langle Y_{2m}^*(\theta, \phi)\rangle \tag{14}$$

where $Y_{2m}(\theta, \phi)$ are the second-order spherical harmonics which are relevant to the interaction. The ensemble average in eq 14 was computed by time-averaging over the whole MD trajectory. Internal correlation functions $C_I(t)$ computed from MD were fitted to eq 12 in the manuscript with the following procedure. First the cost function $X^2 = [C_I(t) - C_I^{ML}(t)]^2$ was minimized over a limited region of the $\{\alpha, \tau, c_{el}\}$ parameter space by a *grid search*, while keeping S^2 fixed to the value S_{MD}^2 computed from MD (see eq 14). Second, the obtained $\{\alpha, \tau, c_{el}\}$ values, together with S_{MD}^2, were used as inputs of a constrained four-parameter X^2 minimization using the so-called bound-constrained "limited memory Broyden–Fletcher–Goldfarb–Shanno" (L-BFGS-B) optimization algorithm.[2] The outcome did not seem to be influenced by the initial values of the parameters.

Relaxation Rate Computation and Fitting. Synthetic quadrupolar ^{2}H and dipolar ^{13}C spin relaxation rates were obtained by using evaluations of the spectral density function $J(\omega)$ based on eq 8 where the fOU parameters (S^2, α, τ_i, c_{el}) obtained from the fitted internal correlation functions were used.[6]

Assuming an axially symmetric electric field gradient around the CD bond, both ^{2}H quadrupolar and ^{13}C ^{1}H dipolar relaxation rates depend on the same spectral density function of the methyl CH (or CD) bond. Thus, the following ^{2}H relaxation rates were simulated according to[32]

$$R_{D_z} = \frac{3}{40}4\pi^2c_Q^2[J(\omega_D) + 4J(2\omega_D)]$$

$$R_{3D_z^2-2} = \frac{3}{40}4\pi^2c_Q^2 \times 3J(\omega_D)$$

$$R_{D_+D_z+D_zD_+} = \frac{4\pi^2}{80}c_Q^2[9J(0) + 3J(\omega_D) + 6J(2\omega_D)]$$

$$R_{D_+} = \frac{4\pi^2}{80}c_Q^2[9J(0) + 15J(\omega_D) + 6J(2\omega_D)]$$

$$R_{D_x^2-D_y^2} = \frac{3}{40}4\pi^2c_Q^2[J(\omega_D) + 2J(2\omega_D)] \tag{15}$$

where $c_Q = (e^2dQ)/\hbar = 167$ kHz is the quadrupolar coulping constant, and the spectral density function $J(\omega)$ is sampled at
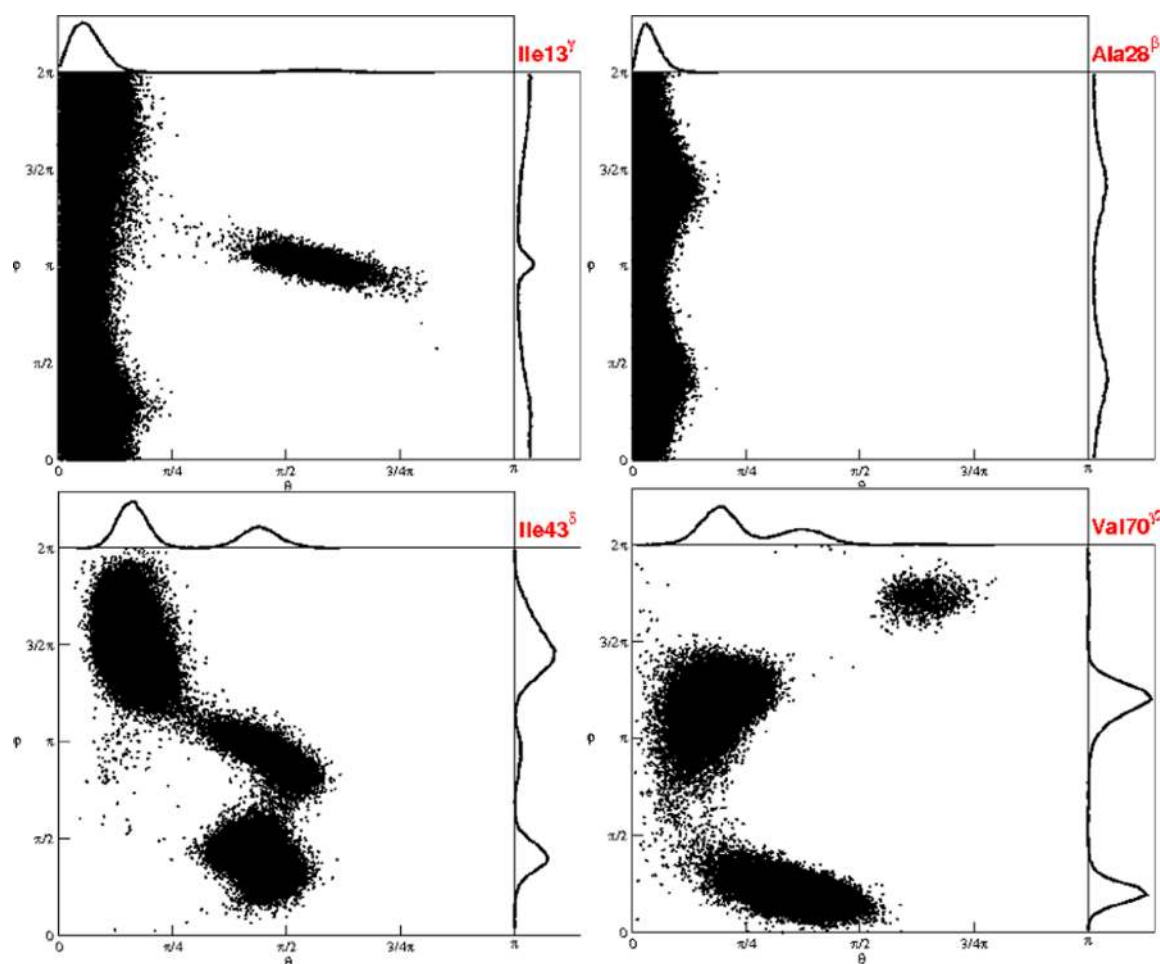
Figure 1. Dot-plots of polar coordinates of CC^γ of residues Ile13 (top left) and CC^β of Ala28 (top right), $C^\gamma C^\delta$ of Ile43 (bottom left) and $C^\beta C'^2$ of Val70 (bottom right) obtained from the MD simulation of ubiquitin. Top and right margins show the histograms of (θ, ϕ) angles in the respective local frames (see text). For Ile13 and Ala28, the respectively unimodal and nearly uniform (θ, ϕ) distributions indicate nearly symmetrical motions about the $\langle \overline{CC} \rangle$ axis. For Ala28, the ϕ distribution is close to uniform despite the presence of two very broad maxima ($\phi \sim \pi/2$ and $\phi \sim 3\pi/2$). The case is similar for CC^γ in Ile13, clearly negligible population in the direction ($\theta \approx \pi/2, \phi \approx \pi$) (see θ histogram). Two major orientations of $C^\gamma C^\delta$ of Ile43 ($\sim \pi/6$; $\sim 3\pi/2$) and ($\sim \pi/3$; $\sim\pi/3$) are observed. This is also the case for $C^\beta C'^2$ of Val70, which also exhibits two main orientations ($\sim \pi/6$; $\sim 5\pi/4$) and ($\sim \pi/3$; $\sim\pi/4$).

frequencies 0, ω_D, and $2\omega_D$. Longitudinal R_1 and NOE ^{13}C relaxation rates were calculated from the expressions

$$R_1 = d_{CH}^2 [J(\omega_H - \omega_C) + 3J(\omega_C) + 6J(\omega_H + \omega_C)]$$
$$+ \frac{\omega_C^2 \Delta \sigma_C^2}{15} 2J(\omega_C)$$

$$\text{NOE} = 1 + \frac{\gamma_H}{\gamma_C} d_{CH}^2 \frac{6J(\omega_H + \omega_C) - J(\omega_H - \omega_C)}{R_1} \quad (16)$$

where γ_H and γ_C are the proton and ^{13}C gyromagnetic ratios, ω_C is the ^{13}C Larmor frequency, and $\hbar = h/2\pi$ is the reduced Planck constant. The CH bond length is denoted by $r_{CH} = 1.115$ A and is assumed constant, and $d_{CH} = (\mu_0/4\pi)((\hbar\gamma_H\gamma_C)/(10r_{CH}^3)^{1/2})$. The chemical shift tensor s is assumed to be axially symmetric with its principal axis along the CH bond, and $\Delta\sigma_C = 25$ ppm denotes the chemical shift anisotropy.

NMR relaxation rates were calculated for a magnetic field $B_0 = 21.1$ T (^{1}H resonance frequency $\nu_0 = 900$ MHz). The overall diffusion correlation time of ubiquitin was set to $\tau_0 = 4.03$ ns.[25] In the case of MMP12, $\tau_0 = 8.27$ ns, which was adapted from ref 24 to the temperature $T = 298$ K of the MD simulations.

Measurement uncertainties were simulated by adding realizations of noise, drawn from a Gaussian distribution $\mathcal{N}(\mu, \sigma)$, to the computed relaxation rates. The standard deviations of each of the MD computed rates were equal to 3% of the rate value, which is typical of experimental measurement. ML parameters were estimated for each realization of the Gaussian noise $\mathcal{N}(\mu, \sigma)$ by minimizing the target function:

$$\chi^2 = \sum_i \sum_{j=1,2} \frac{(R_{ij} - R_{ij}^0)^2}{\sigma_{Rij}^2} \quad (17)$$

where $R_{ij} = R_{1j}$, NOE_j, R_{id_z}, R_{id_x}, $R_{i\,d_{x2}-d_{y2}}$, on the one hand, denote the computed "noisy" relaxation rates at magnetic field B_{0j}, and R_{ij}^0, on the other hand, are the theoretical relaxation rates at the same magnetic field. The associated standard deviations are denoted by σ_{Rij}. Minimization was performed using either a Levenberg–Marquardt algorithm[35] associated with a parameter grid search or the differential evolution method,[38] both implemented in the Scilab software.[8]

III. RESULTS AND DISCUSSION

A. The Effective Potential of Methyl Bond Vectors. The motions of the methyl groups are governed by interactions with
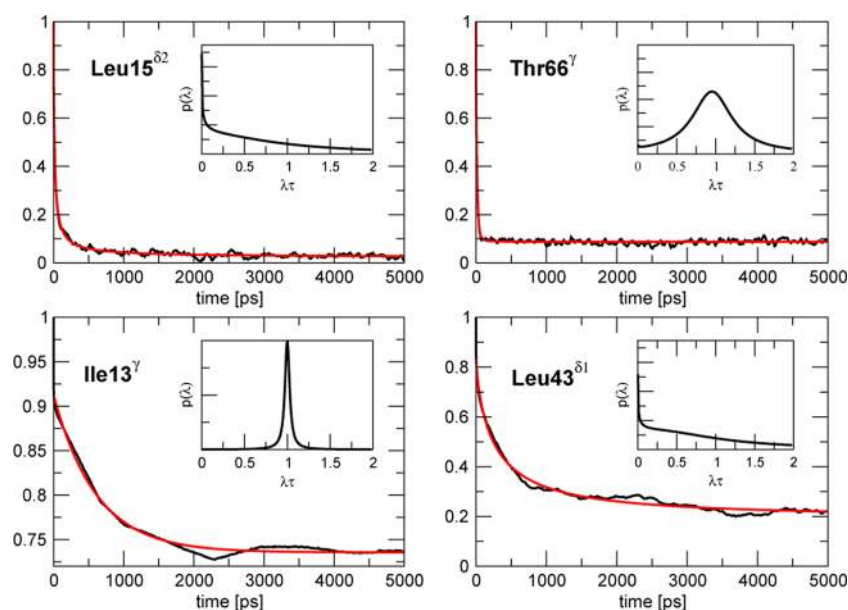
Figure 2. MD-computed $C_I(t)$ and their single ML fitted counterparts showing excellent agreement. CH autocorrelation functions of (top graphics) methyl CH of Leu15$^{\delta_2}$ ($\alpha = 0.70$, $\tau = 26.96$ ps, $c_{el} = 0.84$, $S^2 = 0.020$) and Thr66$^{\gamma}$ ($\alpha = 0.96$, $\tau = 17.13$ ps, $c_{el} = 0.80$, $S^2 = 0.087$) and CC bond vectors of Ile13$^{\gamma}$ ($\alpha = 0.99$, $\tau = 610.65$ ps, $c_{el} = 0.76$, $S^2 = 0.74$) and Leu43$^{\delta 1}$ ($\alpha = 0.70$, $\tau = 354.65$ ps, $c_{el} = 0.85$, $S^2 = 0.18$).

the surrounding molecular environment, which can be accounted for by effective local potentials U_{eff} at the CC and CH bond vectors. These potentials can be related to the population distribution $p_{eq}(\theta, \phi)$ of the polar angles defining the CC (respectively CH) bond vector in a reference frame where z is aligned with $\langle \overrightarrow{CC} \rangle$ (respectively $\langle \overrightarrow{CH} \rangle$) through the expression $p_{eq}(\theta, \phi) \propto e^{-U_{loc}(\theta, \phi)/kT}$. Typical examples of orientation distributions of the bond vectors obtained from our 50 ns MD simulation of ubiquitin are depicted in Figure 1. These illustrate the variety of CC motions: while the methyl groups of certain residues exhibit angular distributions centered on a single orientation (such as CC$^{\gamma}$ and CC$^{\beta}$ of residues Ile13 and Ala28), for several other residues, the presence of multiple preferential directions (C$^{\gamma}$C$^{\delta}$ of Ile43 or C$^{\beta}$C$^{\gamma_2}$ of Val70, for instance) is observed. These translate into single- and multiple-well local potentials. This also indicates that the distinction between harmonic and anharmonic local potentials can be rather fuzzy in practice, and the border between both definitions arbitrary to some extent.

From the NMR spectroscopist viewpoint, it is important to determine the degree to which dynamical complexity can be indeed captured by spin relaxation. Therefore, the internal autocorrelation functions $C_I(t) = \langle P_2(\mathbf{u}(\tau) \cdot \mathbf{u}(0)) \rangle$, of the unit bond vector $\mathbf{u} = \mathbf{u}_{CC}$ or $\mathbf{u}_{CH}$, which are relevant when overall and internal motions of the protein are statistically decorrelated, were computed in both ubiquitin and MMP-12 (see Methods). In this expression, $P_2(.)$ denotes the second Legendre polynomial. Overall, $\approx 70\%$ of CC, and all but one of the CH, bond vector correlation functions, converged to well-defined plateau values (the criteria used to define convergence are detailed in Methods), and were used for subsequent analysis.

Despite the complexity of the local potentials, we investigated the possibility to fit $C_I(t)$ to the model of eq 12 (formally identical to eq 3), characterized by a single ML decay. Surprisingly, the agreement was in general excellent and the single ML decay fully satisfactory, as shown in Figure 2. Different types of behavior of the correlation functions are illustrated for

methyl CH bond vectors of Leu15$^{\delta_2}$ and Thr 66$^{\gamma}$ in ubiquitin (top traces of Figure 2). Interestingly, it is seen that for values of α even slightly different from unity, multiple-scale dynamics[3,4,6] are clearly present, as shown by the rather broad distribution $p_{\alpha,\tau}(\lambda)$ for Thr66$^{\gamma}$ ($\alpha = 0.96$). This therefore demonstrates efficient modeling by a single ML function according to eq 12, even outside of the harmonic potential approximation, and supports the description of the dynamics in terms of an fBD process in a local effective potential. In addition, it is interesting to note that the correlation functions corresponding to residues Leu15$^{\delta_2}$ and Leu43$^{\delta_1}$ are characterized by the same value $\alpha = 0.7$. Thus, the profiles of the associated rescaled densities $p_{\alpha,\tau}(\lambda\tau)$ are identical. However, the τ values are dramatically different, and so are the medians $\lambda_{1/2}$ of $p_{\alpha,\tau}(\lambda)$, since, as mentioned above, $\lambda_{1/2} = \tau^{-1}$.[3] Therefore, although both correlation functions exhibit the same overall shapes, their decays occur with different characteristic times.

For CC correlation functions, wide ranges of α and τ_i values were obtained in ubiquitin ($0.07 \leq \alpha \leq 0.99$ and 11.3 ps $\leq \tau \leq 615.6$ ps) and in MMP-12 ($0.10 \leq \alpha \leq 0.99$ and 0.002 ps $\leq \tau \leq 6037.92$ ps), revealing the dramatic site to site variations of the frequency distribution profile relative to side chain dynamics across the proteins.

For methyl CH, a significant number of values $\alpha \lesssim 0.85$ were obtained ($\sim 14\%$ for ubiquitin and $\sim 20\%$ for MMP-12). These correspond to broad $p_{\alpha,\tau}(\lambda)$ distributions that clearly reflect the nonexponential decay of the correlation functions with asymptotic power law behavior at long times. These findings support the presence of multiple time scale processes, even for such bond motions typically modeled by Markovian very fast jump processes. Moreover, the broad range of (α, τ) parameters illustrates the heterogeneity of methyl group dynamics across the protein as already observed in the case of CC bonds (see Tables S1 and S2), a feature previously noticed for backbone amide NH bond vectors.[4] In this respect, one may raise the question whether CH and CC bond vectors in the same methyl group share common dynamical properties or not. To investigate this point, we plotted the graph of α_{CH} versus α_{CC} (Figure 3). About
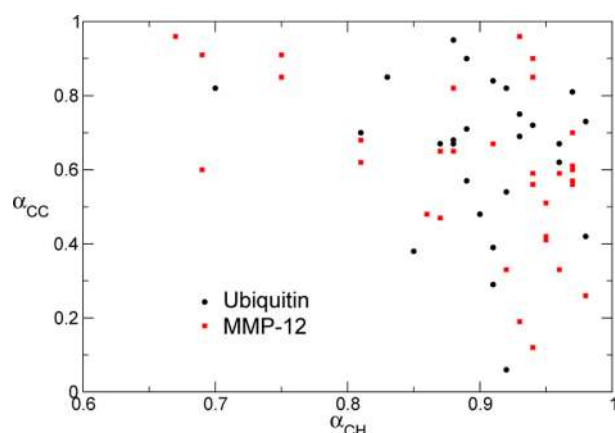
Figure 3. Correlation plot $\{\alpha_{CH}; \alpha_{CC}\}$. Methyl groups with at least one α equal to unity were excluded from this analysis.

80% of the points are located into the region $\alpha_{CH} \gtrsim 0.8$ and $\alpha_{CC} \gtrsim 0.6$ for both ubiquitin and MMP-12, which may therefore be a general property of methyl groups in proteins. No apparent correlation between the two α parameters seems to exist, which suggests that the fractional characteristics of CH bond vectors dynamics are essentially influenced by the closest molecular environment and that their motions are sensitive to different local features. One might expect identical values of α_{CH} and α_{CC} in the unlikely situation of a nonfractional rotational diffusion of the CH3 group, with a fixed CCH angle.

B. Fractal Time Behavior in Multiple-Well Potentials. In order to clarify the conditions of validity of the single ML approximation of the correlation function, and in order to provide better understanding of the fundamental processes in hand, we investigated the bond vector dynamics restricted to motions about each of the potential minima. In addition, determining under what conditions this approximation is acceptable clearly represents a matter with practical implications.

As expected, multiple minima were found for all the CH vectors, which explore at least the three expected preferential directions with $\phi \approx \phi_0 + 2k\pi/3$ upon rotation of the methyl

group. A similar situation is also encountered for numerous methyl CC bond vectors (see Figure 1, where, for residue Ile43$^{\delta}$, one obtained $\alpha = 0.67$ and $\tau = 355$ ps).

The case of CC$^{\gamma_2}$ of residue Val243 in the protein MMP-12 is both interesting and illustrative. The corresponding (θ, ϕ) angular distribution exhibits three preferential orientations defining three minima of the local potential (see Figure S1). Investigation of the dynamical process in hand was performed by analyzing separately the fragments of the MD trajectory relative to the CC bond fluctuations about each of these orientations individually. The internal correlation functions $C_{I(i)}(t)$ of motions about each minimum (i) were computed from the associated fragments of the total trajectory and subsequently averaged in order to reduce statistical errors to values comparable with those of $C_I(t)$ obtained from the whole trajectory. Note that although each substate corresponds to a single minimum of the local potential, its harmonicity is not granted. For this reason, the $C_{I(i)}(t)$ were then fitted to the ML with effective τ_{eff} model (eq 12) for each site independently, yielding a set of $(S^2_{(i)}, c_{el(i)}\alpha_{(i)}, \tau_{eff(i)})$ for each substate. Results are shown in Figure 4. The values of the order parameters calculated for the subconformations were $S^2_{(1)} = 0.83$ and $S^2_{(2)} = 0.84$ and $S^2_{(3)} = 0.86$, respectively. As could be expected, these were much higher values than the $S^2 = 0.05$ characterizing the overall process. In addition, the values of α calculated in these conditions were $\alpha_{(1)} \approx 0.57$, $\alpha_{(2)} \approx 0.58$, $\alpha_{(3)} \approx 0.57$. Interestingly, all of these were rather close to the expected value $\alpha \approx 0.65$ that was determined for the overall process. This is a very important observation, which clearly indicates that the same kind of fractality, as determined by the parameter α, equally characterizes all the potential wells. This therefore shows that same fractional diffusion process is at work in all the minima of the local potential. The associated time constants were found to be $\tau_{eff(1)} = 50.51$ ps, $\tau_{eff(2)} = 128.69$ ps, and $\tau_{eff(3)} = 23.68$ ps. These different, although similar, $\tau_{eff(i)}$ values can be ascribed to the different shapes and depths of the (θ, ϕ) distribution of the CC$^{\gamma_2}$ bond. These values are significantly smaller than $\tau_{eff} = 3.75$ ns obtained by fitting $C_I(t)$ to eq 12, which is also an important observation. Indeed, these results mean that the correlation function for the whole dynamical process contains some of the
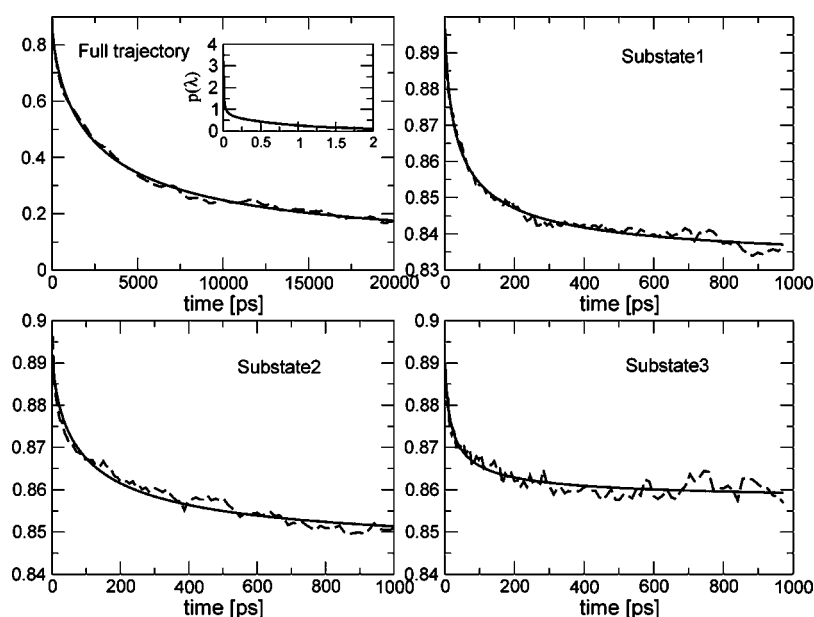

Figure 4. Autocorrelation function of CC bond vector of Val243 in MMP-12 (see text for details).
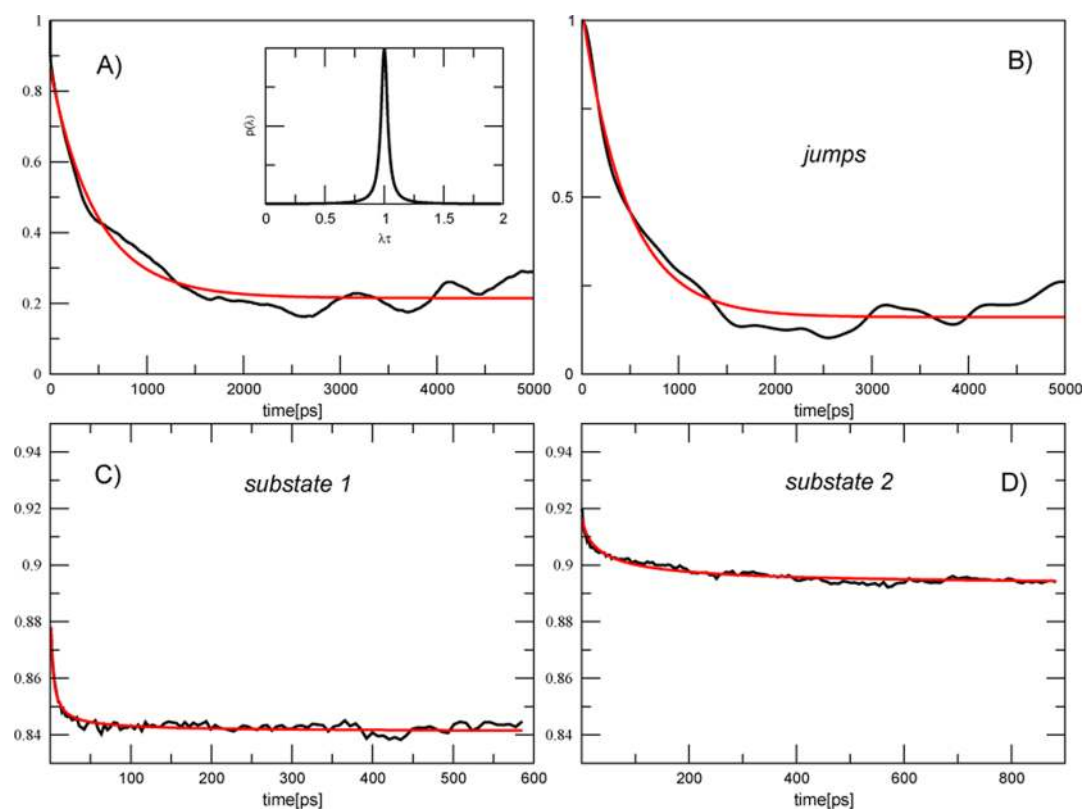
Figure 5. Residue Val70 of ubiquitin. Correlation functions and corresponding fit with fOU model. Top traces: Full 50 ns MD simulation ($\alpha = 0.99$, $\tau = 476$ ps, $S^2 = 0.21$, $c_{el} = 0.86$) and "jumps" between the two substates ($\alpha = 0.99$, $\tau = 463.07$ ps, $S^2 = 0.16$, $c_{el} = 0.82$). Bottom traces: Correlation functions for substates "1" and "2", with parameters ($\alpha = 0.66$, $\tau = 2.40$ ps, $S^2 = 0.84$, $c_{el} = 0.91$) and ($\alpha = 0.61$, $\tau = 47.74$ ps, $S^2 = 0.89$, $c_{el} = 0.92$).

characteristic features of the motions inside the wells, but not all of them. In particular, fitting $C_I(t)$ to an effective fOU model yields a time constant which is absent from the dynamics within the minima. This value τ_{eff} is essentially contributed by the time constant characterizing the fractional transition process *between* the wells. And the fact that the fractional parameter α is nearly identical for all processes attests for the presence of the same stochastic process, albeit in a more complex potential.

From the example above, we propose the following empirical rationale. Here, all three sites can be characterized by nearly identical parameters ($S^2_{(i)}$, $c_{el(i)}\alpha_{(i)}$) and similar time constants $\tau_{eff(i)}$ which, most importantly, are all much smaller than the time constant that characterizes the internal correlation function: $\tau_{eff(i)} \ll \tau_{eff}$. Therefore, the three fast regimes may be associated to a single fast decay of $C_I(t)$ characterized by an effective intrawell mode $\lambda_w \equiv \lambda_{eff(i)}$, while the slower jumps over the potential barriers are accounted for by the slowest relaxation mode λ_1 in eq 9

$$C_I(t) = S^2 + (c_{el} - S^2_w)E_\alpha[-\lambda_w\tau(t/\tau)^\alpha] + (S^2_w - S^2)E_\alpha$$
$$[-\lambda_1\tau(t/\tau)^\alpha] \tag{18}$$

Although eq 18 could be helpful to interpret our data qualitatively, the above analysis shows that the correlation function can be adequately fitted to the model of eq 12, i.e., with a *single* ML function. This thus demonstrates the possibility to actually use the approximate and simplified model of fractional diffusion in an *effective* potential, as suggested so far. It should be emphasized that the presence of two modes is by itself not related to the existence of a fractional diffusion process. Rather, this reflects the presence of potentials with more complex features

than the simple harmonic case. It should be noted that the second term in the rhs of eq 18 can be easily neglected when $c_{el} - S^2_w \ll S^2_w - S^2$, a condition often met in practice for methyl groups. In this case, $C_I(t)$ decays with a (single) rescaled time constant $\tilde{\tau} = (\lambda_1\tau)^{-1/\alpha}\tau$. Interestingly, one therefore retains the actual α, which characterizes the kind of rate constant distribution and the shape of $p_{\alpha,\tau}(\lambda)$ (eq 7). Numerical simulations indicate that this is actually the case for typical conditions, and eq 18 can be fitted by a single ML function to provide the actual α parameter with satisfactory accuracy.

C. Fractionarity of the Apparent Markovian Case. For a number of residues, the values of the fOU model parameters (see Tables S1−4) indicated correlation function characterized by values of $\alpha \sim 1$. This kind of exponential decay, which is in principle indicative of a Markovian process, was in sharp contrast to the fractional Brownian dynamics observed so far and required further investigation. In order to illustrate this point, two such examples are now analyzed in detail.

In the case of the methyl CC bond of residue Val70 in ubiquitin, the (θ, ϕ) angular distribution exhibited two distinct orientations, as attested by the θ and ϕ histograms, which are estimates of their probability density functions and are depicted in the margins of Figure 1. Investigating the dynamics along the same lines as for Val243 in MMP-12, the correlation functions of the "restricted" motions yielded the values $S^2_{(1)} = 0.84$ and $S^2_{(2)} = 0.89$, while the associated values of α were both on the order of $\alpha \approx 0.6$ (see Figure 5) and characteristic of the fractional stochastic process undergone by the bond vector. Again, as noted above, the different shapes of the (θ, ϕ) distribution of the CC$^{\gamma_2}$ bond in Figure 1, therefore of the wells, may explain the different values obtained for the time constants $\tau_{eff(1)} = 2.4$ ps and $\tau_{eff(2)} = 47.7$ ps.
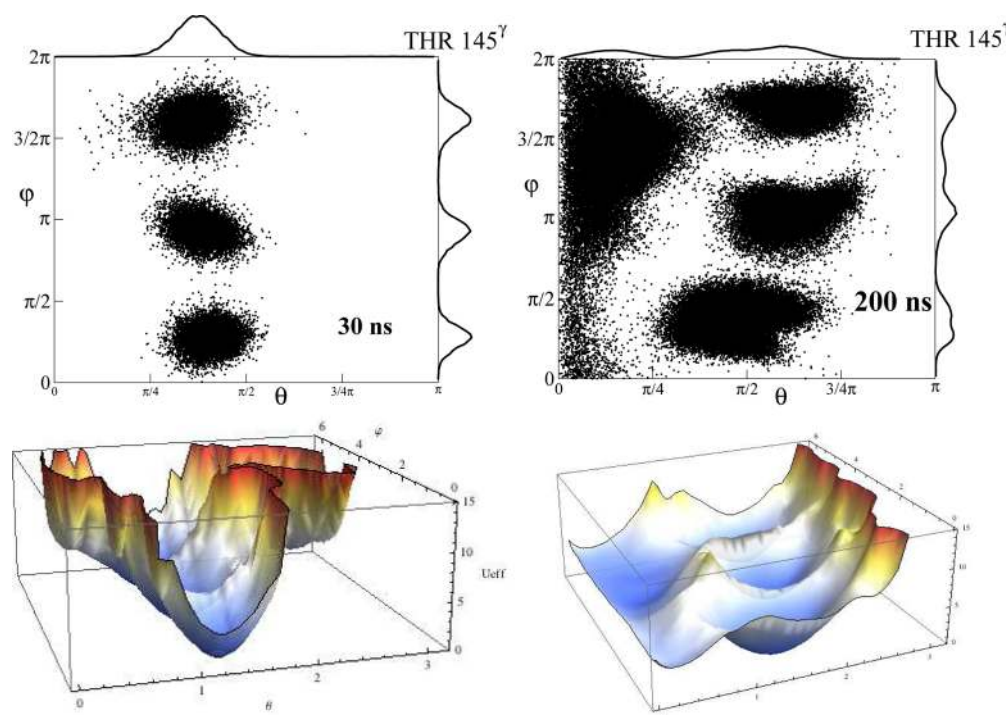
Figure 6. Top: Dot-plots and distributions of (θ, ϕ) angles obtained from partial (30 ns) and total (200 ns) trajectories for Thr145$^\gamma$ in MMP-12. Bottom: Associated local potentials.

A derived stochastic process was obtained by considering only "jumps" between the average directions of the CC bond vector calculated during sojourns in each site independently during the MD trajectory (Figure 5 B). This lead to parameters essentially identical to those of the original process, with $S_J^2 = 0.16$, $\alpha_J = 0.99$, $\tau_J = 463$ ps, and $c_{\mathrm{el\,J}} = 0.92$. Note also that $\tau \approx \tau_J \gg \tau_{\mathrm{eff}(i)}$. However, the value $\alpha_J = 0.99$ is in harsh contrast to the one expected from the analysis of the "intrawell" processes, $\alpha \approx 0.6$. The presence of such conflicting α values was found on several occasions in the simulations, and seemed to be related to the limited length of the MD trajectory. Indeed, in the case of MMP-12, on the order of 50% of the CH bonds associated with $\alpha = 1$ in a 30 ns fragment of the MD simulation were assigned a significant $\alpha < 1$ when the total 200 ns was considered. This is perfectly illustrated in the case of C$^\gamma$H in residue Thr145 in the protein MMP-12. In this case, when only the first 30 ns of the trajectory were used, fitting of the correlation function to eq 3 yielded the value of $\alpha \approx 1$. In contrast, the analysis leads to the value $\alpha = 0.78$ for the whole trajectory (200 ns), thus revealing the signature of the fOU process. In order to get a better insight into this phenomenon, (θ, ϕ) distributions obtained from the partial (30 ns) and total (200 ns) trajectories are plotted in Figure 6. For the shorter trajectory, the distribution of θ is *monomodal* and centered on a value close to the ideal tetrahedral value $\theta = 109.5°$, while the ϕ histogram shows a trimodal distribution about three different values that are separated by 120° and therefore typical of the threefold symmetry of CH$_3$ rotations. Thus, the CH bond samples hardly any intermediate orientation between these. This attests for the much slower time scales on which transitions between these directions of the CH bond occur, as compared to intrawell motions. In contrast, when the total trajectory is analyzed, this simple and ideal three-state feature disappears, and the more complex angle distribution is revealed. Here, the (θ, ϕ) distribution appears broadened, with additional regions significantly populated. The associated local potentials recon-

structed from these trajectories are shown in Figure 6 (bottom traces). Clearly, the simplistic three-well representation of the potential is replaced by a local potential with a more complicated shape, owing to a more extensive sampling of the CH bond orientations. Moreover, for the total 200 ns trajectory, potential barriers between the wells seem lower, which is consistent with a better sampling of processes with long waiting times and the departure from an ideal Kramers kind of problem with a clear-cut separation between the assumed very fast intra-well and the slowest, interwell, modes. Thus, this example illustrates the presence of characteristic times of the stochastic process that are too long to be correctly sampled during the shorter MD simulation.

As will now be shown, this is also related to the misleading $\alpha = 1$ value found in the 30 ns trajectory. These apparent discrepancies are more clearly explained by using an alternative description of fractional diffusion based on the continuous time random walk (CTRW) approach. Here, the diffusing particle evolves according to jumps between nodes located on a grid, where it remains for a random time t before the next jump occurs. This waiting time is characterized by a probability distribution function $\psi(t)$ that decreases for $t \to \infty$ as $\psi(t) \sim (t/\tau)^{-(\alpha+1)}$.[29] The discussion is based on this asymptotic behavior of $\psi(t)$ or, equivalently, of its moment generating function $\hat{\psi}(s)$ (the Laplace transform of $\psi(t)$). Thus, $\hat{\psi}(s) \sim 1 - (\tau s)^\alpha$ for $s \to 0$.[1] When $0 < \alpha < 1$, the first moment of the waiting time probability distribution function diverges, so that $\langle t \rangle = \int_0^\infty t\psi(t)\,\mathrm{d}t = +\infty$. It is shown in this case that when $0 < \alpha < 1$, the process gives rise to the fractional diffusion equation of eq 1. Alternatively, when $\alpha = 1$, $\hat{\psi}(s) \sim 1 - \langle t \rangle s + ...$, which leads to the ordinary Fokker–Planck equation.[1]

In the present context, the issue is whether the long-time tail of the waiting time pdf $\psi(t)$ is sufficiently well sampled during the MD simulation. The answer was so far empirically given by the ability to retrieve a characteristic α parameter strictly lower than
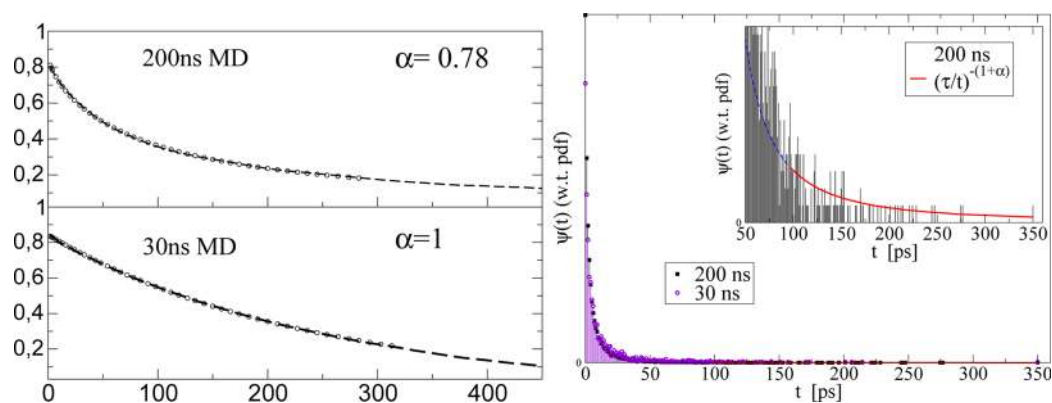
Figure 7. Thr145 of MMP-12. Left: MD-computed (dashed line) and fitted (open circles) correlation functions of the methyl CH bond vector obtained from the first 300 ps of the 30 ns and 200 trajectories. Right: Histogram of the waiting time probability density function $\psi(t)$. The inset shows the superposition with a fit $(\tau/t)^{1+\alpha}$ ($\alpha \approx 0.8$) of the tail of the distribution.
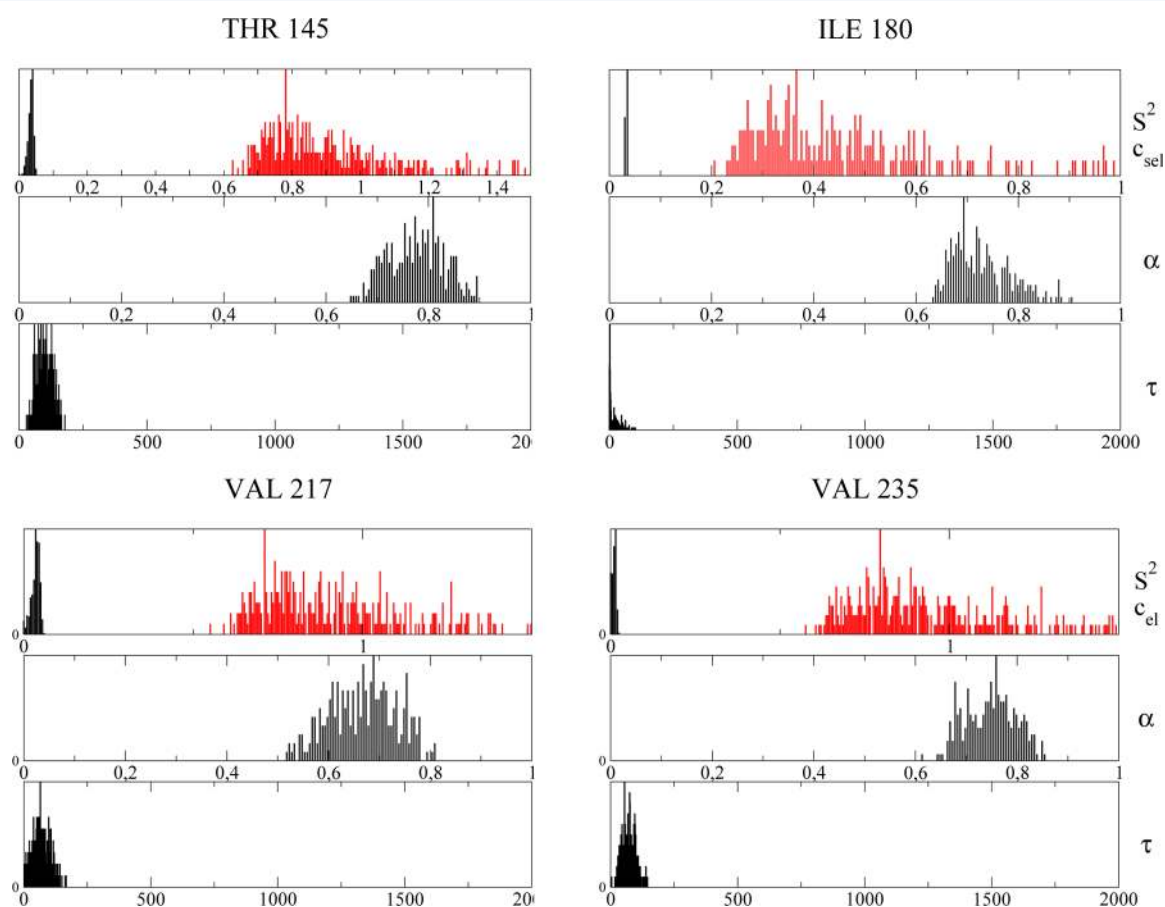

Figure 8. Distribution of $(S^2, c_{el}, \alpha, \tau)$ parameters obtained from Monte Carlo simulations on synthetic NMR relaxation rates from the MD simulation of MMP-12.

unity through fitting the computed $C_I(t)$ to eq 12. This is illustrated in Figure 7, where only the first 300 ps of $C_I(t)$ obtained from the 200 ns and a 30 ns fragment of the MD simulation are fitted, for $C^\gamma H$ in residue Thr145 of MMP-12. Both fits are excellent but provide different values, $\alpha = 0.78$ and $\alpha = 1$. This indicates that the fractional character is recovered only for satisfactory sampling of the stochastic process during the trajectory length.

The largest waiting time that can be in principle sampled at least once during an MD simulation of time duration T_{MD} is precisely T_{MD}. Therefore, in cases where internal correlation

functions with $\alpha < 1$ are obtained, it may be inferred that T_{MD}/τ_{eff} is so large as to allow for good enough sampling of the power law decaying long waiting time tail of $\psi(t)$. If this condition is not met, the resulting truncation of the long time tail of the $\psi(t)$ yields a pdf with a first moment $\langle t \rangle < \infty$, therefore leading to ordinary Brownian diffusion and $\alpha = 1$.

This conjecture was tested for $C^\gamma H$ of Thr145 in MMP-12. To this aim, waiting times were estimated from the trajectory by determining the intervals during which the unitary CH bond vector $\mathbf{u}_{CH}$ did not appreciably change direction. A threshold condition ($\delta|\mathbf{u}_{CH}| \leq 0.3$) was imposed for the minimum

significant norm of the vector change. This condition was set so as to achieve a compromise, since obviously, if this threshold is too low, no large waiting times in the range $[0; T_{MD}]$ occur. The extreme case would be $\delta|\mathbf{u}_{CH}| = 0$, where virtually all the waiting times would be equal to the time step of the simulation. This mainly produces a truncation of $\psi(t)$ for short t, which is not critical for our purpose. Alternatively, too large threshold values of $\delta|\mathbf{u}_{CH}|$ would result in too few jumps occurring during the simulation to allow for a satisfactory estimate of $\psi(t)$ for values of t approaching T_{MD} and to adequately sample the long-time tail of $\psi(t)$. Using this kind of strategy, $\psi(t)$ was then estimated from the histograms of the waiting time values obtained from both the 200 ns MD simulation and a 30 ns fraction thereof. The maximum value of the waiting time $\psi(t)$ and the mean and median of its distribution computed from the 200 ns trajectory were 350, 4, and 9.7 ps, respectively. Alternatively these values became 350, 5, and 12.5 ps for the 30 ns fragment. The "long-time" part of the distribution was then fitted by the power law decay function of the above type. This was achieved by fitting the distribution over 180 ps time intervals and systematically increasing the lower bound. In the case of the 200 ns simulation, values of $\alpha \approx 0.6 \pm 0.2$ were obtained, for intervals with lower bounds comprised between 105 and 134 ps. In any event, these values were close to the one extracted from the correlation function analysis and significantly lower than unity. Moreover, as expected, the fitted $\psi(t) \sim (t/\tau)^{-(\alpha+1)}$ distribution was not consistent with the region of shorter waiting times (see Figure 7). Alternatively, using the same approach, no satisfactory fitting with a $(\tau/t)^{1+\alpha}$ function could be obtained for the 30 ns trajectory.

Thus, these results highlight the connection between the fractional differential equation underlying our analysis of the bond vector correlation functions and the CTRW picture of fractional diffusion. Note that this situation is reminiscent of recent CTRW simulation studies[29] which showed that, although it was due to a different mechanism, the expected time dependence of the ensemble average of the displacement $\langle x^2 \rangle \sim t^{\alpha}$ could not be reproduced by the computed time average $\overline{x^2}$.

D. Methyl Dynamics from NMR Relaxation Rates. In view of practical implementations, we tested the possibility of the fOU model to extract dynamical information from NMR relaxation experiments. So far, our analyses of MD simulations have been supporting the assumption that protein fast internal dynamics is driven by fractional diffusion processes. Therefore the fBD model provides a reasonable tool for the interpretation of experimental data. Specifically, the characterization of the decay rate distribution $p_{\alpha,\tau}(\lambda)$ of the correlation functions (eq 7), which is associated with non-Markovian diffusion with a power law memory kernel, is expected. Thus, a value $\alpha < 1$ obtained from the fitting of the relaxation rates reveals the fractionarity of the underlying diffusion process, therefore its departure from the Markovian case. These indicators are absent from conventional analysis of NMR relaxation data.

To this aim, in analogy with a recent study,[6] synthetic NMR ^{2}H and ^{13}C relaxation rates were computed from the spectral density function of eq 8 with $(S^2, c_{el}, \alpha, \tau)$ parameters fitted from MD correlation functions. Model parameters could be extracted by Monte Carlo simulations on synthetic relaxation rates with pseudoexperimental noise. Statistical properties of the fitted values could be estimated from the obtained distribution of values, and the associated medians were found in satisfactory agreement with the values determined from the MD angular

autocorrelation functions of CH bond vectors (see Tables S1−4). Illustrative examples are shown in Figure 8. The three parameters S^2, α, and τ are extracted with relatively modest dispersion about their medians, although c_{el} parameters exhibit larger spread, with a significant number of them lying outside the range of physically acceptable values. It is interesting to compare these results with ones obtained previously on ^{15}N amide backbone relaxation rates.[6] There, it was shown that the smaller the difference between parameters c_{el} and S^2, the larger the dispersion of α and τ, which was ascribed to less favorable fitting configurations of the parameters. This is quite different for the present case where the S^2-order parameters of CH correlation functions are often very low (i.e., lower than approximately 0.1).

From the model parameters α and τ, and within the effective relaxation time approximation ($\tau = \tau_{eff}$), it is then possible to reconstruct the relaxation rate distribution function $p_{\alpha,\tau}(\lambda)$, which actually defines a distribution of time scales and completely characterizes the fractional diffusion process with memory kernel $K(t) = ((\alpha-1)/(\tau^2\Gamma(\alpha)))(t/\tau)^{\alpha-2}$.[21]

Overall, the present study suggests that the multiscale character of the stochastic process embodied in the value of α can be extracted from relaxation measurements, thereby providing insight into the structure of the underlying random process.

IV. CONCLUSION

In the present study, the multiscale character of the stochastic process underlying methyl dynamics in proteins has been characterized based on the analysis of MD simulations. In addition to the important parametrization of the internal correlation functions by functions of the Mitag−Leffler type, the connection between average properties embedded in the correlation functions and the stochastic process, which is characterized by the waiting time pdf associated to the process, was demonstrated. Therefore, the approach described in this work provides an important conceptual advance that should be particularly useful in dealing with actual measurements, by providing renewed insight into the interpretation of NMR relaxation data.

■ ASSOCIATED CONTENT

Ⓢ Supporting Information

Additional tables and figures as described in the text. This material is available free of charge via the Internet at http://pubs.acs.org.

■ AUTHOR INFORMATION

Corresponding Author

*E-mail: daniel.abergel@ens.fr (D.A.).

Notes

The authors declare no competing financial interest.

■ ACKNOWLEDGMENTS

■ REFERENCES

(1) Barkai, E.; Metzler, R.; Klafter, J. From continuous time random walks to the fractional Fokker−Planck equation. *Phys. Rev. E* **2000**, *61*, 132−138.

(2) Byrd, R. H.; Lu, P.; Nocedal, J.; Zhu, C. A limited memory algorithm for bound constrained optimization. *SIAM J. Sci. Comput.* **1995**, *16*, 1190−1208.

(3) Calandrini, V.; Abergel, D.; Kneller, G. Protein dynamics from NMR perspective: Network of coupled rotators and fractional Brownian dynamics. *J. Chem. Phys.* **2008**, *128*, 145102−8.

(4) Calandrini, V.; Abergel, D.; Kneller, G. Fractional protein dynamics seen by nuclear magnetic resonance spectroscopy: Relating molecular dynamics simulation and experiment. *J. Chem. Phys.* **2010**, *133*, 145101−9.

(5) Calandrini, V.; Pellegrini, E.; Calligari, P.; Hinsen, K.; Kneller, G. nMoldyn-interfacing spectroscopic experiments, molecular dynamics simulations and models for time correlation functions. *Collect. SFN* **2011**, *12*, 201−232.

(6) Calligari, P.; Calandrini, V.; Kneller, G. R.; Abergel, D. From NMR relaxation to fractional Brownian dynamics in proteins: Results from a virtual experiment. *J. Phys. Chem. B* **2011**, *115* (43), 12370−9.

(7) Chatfield, D. C.; Szabo, A.; Brooks, B. R. Molecular dynamics of staphylococcal nuclease: Comparison of simulation with 15N and 13C NMR relaxation data. *J. Am. Chem. Soc.* **1998**, *120*, 5301−5311.

(8) Consortium, S. *Scilab: Free and Open Source software for numerical computation*; Scilab Consortium, Digiteo, Paris, France, 2011.

(9) Cote, Y.; Senet, P.; Delarue, P.; Maisuradze, G. G.; Scheraga, H. A. Nonexponential decay of internal rotational correlation functions of native proteins and self-similar structural fluctuations. *Proc. Natl. Acad. Sci. U.S.A.* **2010**, *107*, 19844−19849.

(10) Darden, T.; York, D.; Pedersen, L. Particle mesh Ewald: An n log(n) method for Ewald sums in large systems. *J. Chem. Phys.* **1993**, *98*, 10089−10092.

(11) Erdélyi, A.; Magnus, W.,; Oberhettinger, F.; Tricomi, F. *Higher Transcendental Functions*; McGraw Hill: New York, 1995.

(12) Essmann, U.; Perera, L.; Berkowitz, M.; Darden, T.; Lee, H.; Pedersen, L. A smooth particle mesh Ewald method. *J. Chem. Phys.* **1995**, *103*, 8577−8593.

(13) Feller, S.; Zhang, Y.; Pastor, R.; Brooks, B. Constant-pressure molecular-dynamics simulation—The Langevin piston method. *J. Chem. Phys.* **1995**, *103* (11), 4613−4621.

(14) Glöckle, W.; Nonnenmacher, T. A fractional calculus approach to self-similar protein dynamics. *Biophys. J.* **1995**, *68*, 46−53.

(15) Hornak, V.; Abel, R.; Okur, A.; Strockbine, B.; Roitberg, A.; Simmerling, C. Comparison of multiple amber force fields and development of improved protein backbone parameters. *Proteins* **2006**, *65* (3), 712−725.

(16) Igumenova, T. I.; Frederick, K. K.; Wand, A. J. Spin relaxation processes in a two-proton system undergoing anisotropic reorientation. *Chem. Rev.* **2006**, *106*, 1672−1699.

(17) Izaguirre, J.; Catarello, D.; Wozniak, J.; Skeel, R. Langevin stabilization of molecular dynamics. *J. Chem. Phys.* **2001**, *114*, 2090−2098.

(18) Jarymowicz, V. A.; Stone, M. Fast time scale dynamics of protein backbones: NMR relaxation methods, applications, and functional consequences. *Chem. Rev.* **2006**, *106*, 1624−1671.

(19) Kalmykov, Y. P. Fractional rotational Brownian motion in a uniform dc external field. *Phys. Rev. E* **2004**, *70*, 051106−7.

(20) Kneller, G. Quasielastic neutron scattering and relaxation processes in proteins: Analytical and simulation-based models. *Phys. Chem. Chem. Phys.* **2005**, *7*, 2641−2655.

(21) Kneller, G.; Hinsen, K. Fractional Brownian dynamics in proteins. *J. Chem. Phys.* **2004**, *121*, 10278−10283.

(22) Kou, S.; Xie, X. Generalized Langevin equation with fractional gaussian noise: Subdiffusion within a single protein molecule. *Phys. Rev. Lett.* **2004**, *93*, 180603−4.

(23) Lee, A.; Flynn, P.; Wand, A. Comparison of 2H and 13C NMR relaxation techniques for the study of protein methyl group dynamics in solution. *J. Am. Chem. Soc.* **1999**, *121* (12), 2891−2902.

(24) Liang, X.; Arunima, A.; Zhao, Y.; Bhaskaran, R.; Shende, A.; Byrne, T. S.; Fleeks, J.; Palmier, M. O.; Doren, S. R. V. Apparent tradeoff of higher activity in MMP-12 for enhanced stability and flexibility in MMP-3. *Biophys. J.* **2006**, *99*, 273−283.

(25) Lienin, S.; Bremi, T.; Brutscher, B.; Brüschweiler, R.; Ernst, R. Anisotropic intramolecular backbone dynamics of ubiquitin characterized by NMR relaxation and MD computer simulation. *J. Am. Chem. Soc.* **1998**, *120*, 9870−9879.

(26) Lipari, G.; Szabo, A. Model-free approach to the interpretation of nuclear magnetic resonance relaxation in macromolecules. 1. Theory and range of validity. *J. Am. Chem. Soc.* **1982a**, *104* (17), 4546−4559.

(27) Lipari, G.; Szabo, A. Model-free approach to the interpretation of nuclear magnetic resonance relaxation in macromolecules. 2. Analysis of experimental results. *J. Am. Chem. Soc.* **1982b**, *104* (17), 4559−4570.

(28) Lu, H.; Xun, L.; Xie, X. S. Single-molecule enzymatic dynamics. *Science* **1998**, *282*, 1877−1882.

(29) Lubelski, A.; Sokolov, I.; Klafter, J. Nonergodicity mimics inhomogeneity in single particle tracking. *Phys. Rev. Lett.* **2008**, *100*, 250602−4.

(30) Mackerell, A. D., Jr.; Feig, M.; Brooks, C. L. Extending the treatment of backbone energetics in protein force fields: Limitations of gas-phase quantum mechanics in reproducing protein conformational distributions in molecular dynamics simulations. *J. Comput. Chem.* **2004**, *25*, 1400−15.

(31) Metzler, R.; Klafter, J. The random walk's guide to anomalous diffusion: A fractional dynamics approach. *Phys. Rep.* **2000**, *339*, 1−77.

(32) Millet, O.; Muhandiram, D. R.; Skrynnikov, N. R.; Kay, L. E. Deuterium spin probes of side-chain dynamics in proteins. 1. Measurement of five relaxation rates per deuteron in (13)C-labeled and fractionally (2)H-enriched proteins in solution. *J. Am. Chem. Soc.* **2002**, *124* (22), 6439−6448.

(33) Nederveen, A. J.; Bonvin, A. M. J. J. NMR relaxation and internal dynamics of ubiquitin from a 0.2 μs MD simulations. *J. Chem. Theory Comput.* **2005**, *1*, 363−374.

(34) Phillips, J.; Braun, R.; Wang, W.; Gumbart, J.; Tajkhorshid, E.; Villa, E.; Chipot, C.; Skeel, R.; Kale, L.; Schulten, K. Scalable molecular dynamics with namd. *J. Comput. Chem.* **2005**, *26* (16), 1781−1802.

(35) Press, W. H.; Flannery, B. P.; Teukolsky, S.; Vetterling, W. T. *Numerical Recipes*; Cambridge University Press: New York, 1989.

(36) Shlesinger, M. F.; Montroll, E. W. On the Williams−Watts function of dielectric relaxation. *Proc. Natl. Acad. Sci. U.S.A.* **1984**, *81*, 1280−1283.

(37) Skrynnikov, N. R.; Millet, O.; Kay, L. E. Deuterium spin probes of side-chain dynamics in proteins. 2. Spectral density mapping and identification of nanosecond time-scale side-chain motions. *J. Am. Chem. Soc.* **2002**, *124* (22), 6449−6460.

(38) Storn, R.; Price, K. Differential evolution: A simple and efficient heuristic for global optimization over continuous spaces. *J. Glob. Optim.* **1997**, *11*, 341−359.

(39) Zwanzig, R.; Ailawadi, N. Statistical error due to finite time averaging in computer experiments. *Phys. Rev.* **1969**, *182* (1), 280−283.